



UNIVERSITY OF LEEDS

This is a repository copy of *Functional integrity of the contractile actin cortex is safeguarded by multiple Diaphanous-related formins*.

White Rose Research Online URL for this paper:  
<http://eprints.whiterose.ac.uk/140860/>

Version: Accepted Version

---

**Article:**

Litschko, C, Brühmann, S, Csiszár, A et al. (12 more authors) (2019) Functional integrity of the contractile actin cortex is safeguarded by multiple Diaphanous-related formins. *Proceedings of the National Academy of Sciences of the United States of America*, 116 (9). pp. 3594-3603. ISSN 0027-8424

<https://doi.org/10.1073/pnas.1821638116>

---

© 2019, Published under the PNAS license. This is an author produced version of a paper published in *Proceedings of the National Academy of Sciences of the United States of America*. Uploaded in accordance with the publisher's self-archiving policy.

**Reuse**

Items deposited in White Rose Research Online are protected by copyright, with all rights reserved unless indicated otherwise. They may be downloaded and/or printed for private study, or other acts as permitted by national copyright laws. The publisher or other rights holders may allow further reproduction and re-use of the full text version. This is indicated by the licence information on the White Rose Research Online record for the item.

**Takedown**

If you consider content in White Rose Research Online to be in breach of UK law, please notify us by emailing [eprints@whiterose.ac.uk](mailto:eprints@whiterose.ac.uk) including the URL of the record and the reason for the withdrawal request.



[eprints@whiterose.ac.uk](mailto:eprints@whiterose.ac.uk)  
<https://eprints.whiterose.ac.uk/>

# Functional integrity of the contractile actin cortex is safeguarded by multiple Diaphanous-related formins

Christof Litschko<sup>1</sup>, Stefan Brühmann<sup>1</sup>, Agnes Csiszár<sup>2</sup>, Till Stephan<sup>1</sup>, Vanessa Dimchev<sup>3</sup>, Julia Damiano-Guercio<sup>1</sup>, Alexander Junemann<sup>1</sup>, Sarah Körber<sup>1</sup>, Moritz Winterhoff<sup>1</sup>, Benjamin Nordholz<sup>1</sup>, Nagendran Ramalingam<sup>4</sup>, Michelle Peckham<sup>5</sup>, Klemens Rottner<sup>3</sup>, Rudolf Merkel<sup>2</sup>, Jan Faix<sup>1</sup>

<sup>1</sup>Hannover Medical School, <sup>2</sup>Forschungszentrum Jülich GmbH, <sup>3</sup>Technische Universität Braunschweig, <sup>4</sup>Harvard Medical School, <sup>5</sup>University of Leeds

Submitted to Proceedings of the National Academy of Sciences of the United States of America

The contractile actin cortex is a thin layer of filamentous actin, myosin motors and regulatory proteins beneath the plasma membrane crucial to cytokinesis, morphogenesis and cell migration. However, the factors regulating actin assembly in this compartment are not well understood. Using the *Dictyostelium* model system, we show that the three Diaphanous-related formins (DRFs) ForA, ForE and ForH are regulated by the RhoA-like GTPase RacE and synergize in the assembly of filaments in the actin cortex. Single or double formin-null mutants displayed only moderate defects in cortex function whereas the concurrent elimination of all three formins or of RacE caused massive defects in cortical rigidity and architecture as assessed by aspiration assays and electron microscopy. Consistently, the triple formin- and RacE-mutants encompassed large peripheral patches devoid of cortical F-actin and exhibited severe defects in cytokinesis and multicellular development. Unexpectedly, many *forA*/*H*/*E* and *racE*-mutants protruded efficiently, formed multiple exaggerated fronts and migrated with morphologies reminiscent of rapidly-moving fish keratocytes. In 2D-confinement, however, these mutants failed to properly polarize and recruit myosin II to the cell rear essential for migration. Cells arrested in these conditions displayed dramatically amplified flow of cortical actin filaments, as revealed by TIRF-imaging and iterative particle image velocimetry (PIV). Consistently, individual and combined, CRISPR/Cas9-mediated disruption of genes encoding mDia1 and -3 formins in B16-F1 mouse melanoma cells revealed enhanced frequency of cells displaying multiple fronts, again accompanied by defects in cell polarization and migration. These results suggest evolutionarily conserved functions for formin-mediated actin assembly in actin cortex mechanics.

actin cortex | formin | RhoGTPase | cell migration | cytokinesis

## Introduction

The actin-rich cell cortex is required for cell shape remodeling in fundamental cellular processes such as cytokinesis, morphogenesis and cell migration (1). Cell motility is regulated by polarization, adhesion and cytoskeletal activities leading to site-specific force generation, as exemplified by leading edge actin assembly and myosin-dependent rear contraction (2–4). Based on considerable variations of these activities in different cell types, this process is further subdivided into mesenchymal and amoeboid types of migration as two extremes of a wide spectrum (5). The slow mesenchymal type of motility is characterized by strong substrate adhesion and formation of prominent stress fibers as well as a protruding lamellipodium at the front (6), whereas fast amoeboid migration as exemplified by *Dictyostelium* cells is defined by weaker and more transient adhesions, a rounder cell shape, actin-rich protrusions or blebs in the front and myosin-driven contraction in the rear (7, 8). However, migration and other processes involving cell shape remodeling as e.g. cytokinesis also require a thin, actin-rich cortex below the membrane.

This cortex contains actin, myosin and associated factors assembling into a multi-component layer (9, 10), which is intimately linked to the membrane in a PI(4,5)P<sub>2</sub>-dependent manner by the

ezrin, radixin and moesin (ERM)-family of proteins in animal cells (11, 12) and cortexillin (Ctx) in *Dictyostelium* (13–15). The function of this thin actin meshwork is comparable to cell walls in plants, yeast and bacteria, as it defines the cell's stiffness, resists external forces and counteracts intracellular, hydrostatic pressure (9, 16). However, as opposed to the static cell wall of plants and bacteria, the actin cortex of amoebae and animal cells has viscoelastic properties that can be remodeled in the timescale of seconds. Rapid F-actin rearrangements enable cells to promptly modify their shapes for fast adaptation to changes in extracellular environment (9, 16). Moreover, and as opposed to cells with rigid cell walls engaging them entirely, cell cortex constituents of motile eukaryotic cells are organized in gradients due to the asymmetry of positioning signals (17).

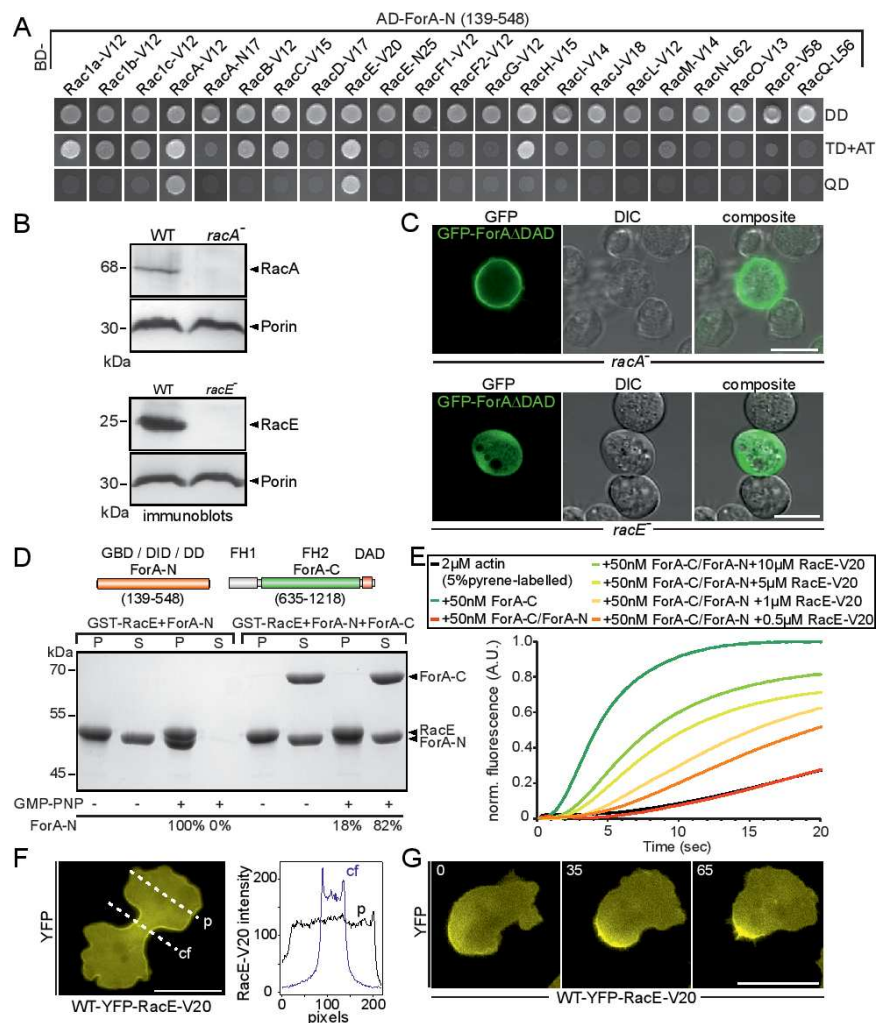
The physical properties of the cell cortex such as its tension and contractility likely impacting on plasma membrane dynamics are regulated by myosin motor activity as well as the arrangement and density of F-actin networks generated by distinct actin-assembly machineries (9). In cells, actin polymerization is mostly initiated by Arp2/3 complex and formins (18). The Arp2/3 complex creates branches at the sides of preexisting mother filaments and generates a dense actin meshwork at the front of migrating cells (18, 19). Formins instead nucleate and elongate long and linear actin filaments (19). A major subgroup of the formin family is comprised by Diaphanous-related formins (DRFs), which are autoinhibited due to intramolecular interactions of the Diaphanous

## Significance

The actin-rich cell cortex is a viscoelastic structure participating in a variety of cellular processes. However, the complete inventory of actin assembly factors driving its formation and knowledge about their specific contributions is still incomplete. We show here that functional integrity of the cell cortex in *Dictyostelium* and mammalian cells is backed up by multiple Diaphanous-related formins that are regulated by Rho-subfamily GTPases. These DRFs contribute to the generation of long actin filaments of the contractile actin cortex and are required for cell mechanics. Of note, these factors are excluded from Arp2/3 complex-nucleated networks, implying diversification of the cortex into functional subcompartments to segregate cortical actomyosin contraction in the rear or cleavage furrow ingression from actin-based protrusion in the front.

## Reserved for Publication Footnotes

137  
138  
139  
140  
141  
142  
143  
144  
145  
146  
147  
148  
149  
150  
151  
152  
153  
154  
155  
156  
157  
158  
159  
160  
161  
162  
163  
164  
165  
166  
167  
168  
169  
170  
171  
172  
173  
174  
175  
176  
177  
178  
179  
180  
181  
182  
183  
184  
185  
186  
187  
188  
189  
190  
191  
192  
193  
194  
195  
196  
197  
198  
199  
200  
201  
202  
203  
204



205  
206  
207  
208  
209  
210  
211  
212  
213  
214  
215  
216  
217  
218  
219  
220  
221  
222  
223  
224  
225  
226  
227  
228  
229  
230  
231  
232  
233  
234  
235  
236  
237  
238  
239  
240  
241  
242  
243  
244  
245  
246  
247  
248  
249  
250  
251  
252  
253  
254  
255  
256  
257  
258  
259  
260  
261  
262  
263  
264  
265  
266  
267  
268  
269  
270  
271  
272

**Fig. 1.** ForA is regulated by the RhoA-homologue RacE. (A) The N-terminal domain of ForA (ForA-N) containing the GBD interacts specifically with the activated forms of RacA (RacA-V12) and RacE (RacE-V20) in the Y2H assay. Yeast was transformed with the indicated constructs and selected for the presence of prey and bait plasmids by growth on double-dropout (DD) media lacking leucine and tryptophan. Interactions were assayed by growth on stringent triple-dropout (TD) media additionally lacking histidine in the presence of 3 mM 3-AT and on quadruple-dropout (QD) media additional lacking histidine and adenine. AD, Gal4-activation domain; 3-AT, 3-amino-1,2,4-triazole; (B) Genetic elimination of RacA and RacE was confirmed by immunoblotting. Porin was used as a loading control. (C) Constitutively active ForA fused to GFP requires RacE for targeting to the cell cortex but localizes appropriately in the absence of RacA. Scale bars, 10  $\mu$ m. (D) ForA constructs used for biochemical analyses. GBD, GTPase-binding domain; DID, diaphanous inhibitory domain; DD, dimerization domain; FH, formin homology domain; DAD, diaphanous autoinhibitory domain. Active RacE interacts directly with ForA-N and was able to partially release ForA-N from the autoinhibited ForA-N/ForA-C complex. GST-pulldown experiments with GMPPNP-loaded RacE are shown. (P) pellet; (S) supernatant. The numbers below indicate the relative amounts of ForA-N in P and S fractions. (E) Active RacE releases autoinhibition of the catalytically inactive ForA-N/ForA-C complex to promote actin assembly in pyrene assays in a concentration-dependent manner. (F) Active RacE N-terminally fused to YFP accumulates about 2-fold in the cell cortex of the cleavage furrow in 2D-confinement under agar. Abbreviations: cf, cleavage furrow; p, pole. Scale bar, 20  $\mu$ m. (G) Images from lime-lapse movies correspond to Movie S1 and show that active RacE is enriched in the rear cell cortex of a polarized cell migrating under agar. Scale bar, 20  $\mu$ m.

inhibitory domain (DID) with the Diaphanous autoregulatory domain (DAD) (20). DRF autoinhibition is commonly released by binding of activated Rho-family GTPases (21, 22), but can also be driven by Ras (23). As yet, both Arp2/3 complex and formins have been implicated in the generation of cortical actin in different cell types (24, 25). However, the precise quantitative contributions of Arp2/3 complex- and formin- generated filaments to this structure and their interplay in cortical functions are still elusive. Depletion of the formin mDia1 (Diaph1) in HeLa cells led to failure of cortex function in mitotic cell division, while depletion of Arp2/3 complex alone did not (24). Interestingly, the same study reported Arp2/3 complex inhibition to potentiate effects of mDia1 depletion, suggesting synergistic activities of mDia1 and Arp2/3 complex in the nucleation of cortical actin (24). AFM measurements indicated that cortical elasticity in HeLa and M2

melanoma cells is mostly affected by the formin inhibitor SmiFH2 (25). In contrast, reducing Arp2/3 complex activity by CK666 did not appear to play a critical role (25). These data suggested central roles for formins in cell cortex mechanics, but need to be complemented by genetics, last not least to identify specific, contributing formins.

Previously, we established that the mDia1-related formin ForA in *Dictyostelium* cells prevents blebbing in the rear to assist protrusion at the front, in particular under mechanical stress (18). Here, we identify and characterize two additional mDia-related, cortical *Dictyostelium* formins, ForE and ForH, which synergize with ForA to safeguard cortex-dependent functions. Moreover, we extend our studies to mammalian formins mDia1 and -3, providing conclusive evidence that comparable pathways operate in higher eukaryotes.

273  
274  
275  
276  
277  
278  
279  
280  
281  
282  
283  
284  
285  
286  
287  
288  
289  
290  
291  
292  
293  
294  
295  
296  
297  
298  
299  
300  
301  
302  
303  
304  
305  
306  
307  
308  
309  
310  
311  
312  
313  
314  
315  
316  
317  
318  
319  
320  
321  
322  
323  
324  
325  
326  
327  
328  
329  
330  
331  
332  
333  
334  
335  
336  
337  
338  
339  
340

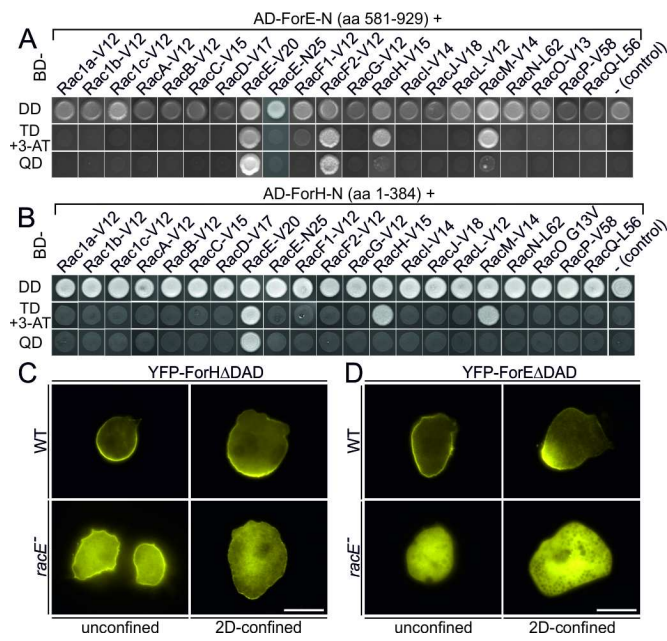


**Fig. 2.** Active RacE interacts with two additional cortical formins. (A-B) ForE-N and ForH-N interact specifically with the active form of RacE (V20) in the Y2H assay. Yeast was transformed with the indicated constructs and selected for the presence of prey and bait plasmids by growth on double-dropout (DD) media lacking leucine and tryptophan. ForE-N additionally showed strong interaction with active RacF2 (V12). Interactions were scored by growth on stringent triple-dropout (TD) media in the presence of 3 mM 3-AT or quadruple-dropout (QD) media as outlined in Fig. 2. Both formins showed no genetic interaction using the dominant-negative RacE (N25) variant or empty AD plasmids as negative controls. AD, Gal4-activation domain; 3-AT, 3-amino-1,2,4-triazole; BD, Gal4-binding domain. (C-D) Constitutively active ForE and ForH localize in the cell cortex and rear of migrating WT cells. YFP-tagged variants of the formins were expressed in WT and *racE* cells and analyzed by wide-field fluorescence microscopy at the conditions indicated. Scale bars, 10  $\mu$ m.

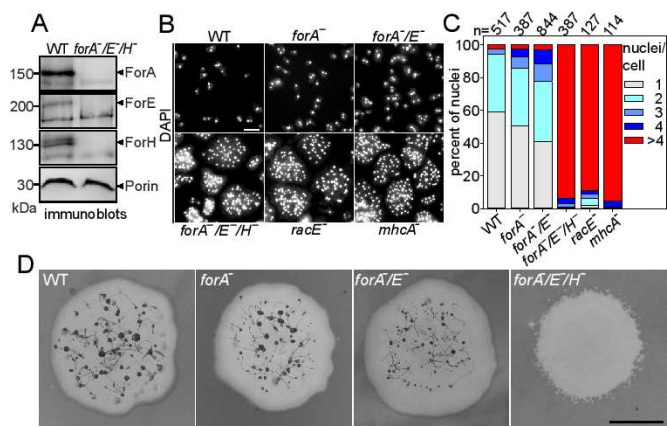


**Fig. 3.** Elimination of all three cortical formins is detrimental for cell division and development. (A) Inactivation of the *forA*, *forE* and *forH* genes in the triple knockout mutant was verified by immunoblotting using specific formin sera. Porin was used as a loading control. (B) WT and the mutant cells indicated were grown for 48 h in shaken suspension at 150 rpm, subsequently seeded on glass cover slips, fixed and stained with DAPI to visualize the nuclei. Scale bar, 20  $\mu$ m. (C) Quantification of nuclei in cells as shown in (B). n, number of analyzed cells. (D) Coincident elimination of ForA, ForE and ForH blocks development. WT or formin-deficient cells were transferred with a tooth pick onto a lawn of *K. aerogenes* on non-nutrient agar plates and monitored after 96-120 h of development. Scale bar, 0.5 mm.

**Results**

**Active ForA accumulates in the cleavage furrow of dividing cells.** Consistent with the mechanistic similarities between migration and cytokinesis, many proteins accumulating in the trailing edge, as for instance myosin II, cortaxillin (Ctx), the functional homologue of ERM proteins in *Dictyostelium*, and IQGAPs, were also found in cleavage furrows and are known to regulate cytokinesis (26–28). Thus, we explored the localization of active ForA at different stages of the cell cycle. Active ForA is uniformly localized in the cell cortex of unpolarized interphase cells (17). In mitotic cells, active ForA remained evenly distributed in the cell cortex up to early anaphase, but subsequently began to relocalize to the cleavage furrow like IQGAP1 and Ctx I ("SI Appendix, Fig. S1 A and B"), strongly suggesting a critical function of formin-generated cortical actin in cytokinesis, as previously shown in a variety of cell types (29). However, when cultivated in petri dishes allowing adhesion of cells to the substratum, or even when exposed to high shear forces in shaken suspension culture, *forA* cells exhibited negligible defects in cytokinesis ("SI Appendix Fig. S1 C and D"). Of note, we have previously shown that either Ctx I and II or IQGAP1 and IQGAP2 had to be eliminated simultaneously to cause strong defects in cytokinesis, while single knockout mutants exhibited no or minor defects (28). Thus, the lack of a cytokinesis defect in *forA* cells suggested functional overlaps of ForA with one or multiple other cortical formins to safeguard this critical cellular function. In line with this view, cortical F-actin is still present in contractile regions of *forA* cells, such as the trailing edge (17).

**ForA interacts with active form of the RhoA homologue RacE.** DRFs such as ForA are commonly assumed to be activated by GTP-bound Rho-family GTPases. *Dictyostelium* cells lack canonical Cdc42 and Rho homologues, but express 20 Rac proteins, some of which exert characteristics of Cdc42 and RhoA functions. Since appropriate ForA targeting and activation requires concurrent interactions with PI(4,5)P2 and an active GTPase (17), we employed yeast-two-hybrid (Y2H) analyses to systematically screen all 20 *Dictyostelium* Racs for interaction with the N-terminal domain of ForA encompassing the GBD. Under the most stringent growth conditions on selective media, ForA genetically interacted with constitutively active RacA and RacE, while it failed to interact with dominant-negative variants of these GTPases (Fig. 1A). RacA has not yet been characterized, but contains a BTB domain at its C-terminus and lacks a classical CAAX motive required for prenylation (30). Consistently, ectopically expressed RacA fused to GFP localized ubiquitously in the cytoplasm and was not enriched at the cell cortex (Fig. S2). Thus, it appeared unlikely that it regulates recruitment and activation of ForA at the cortex. RacE instead was previously implicated in regulation of cortical tension and cleavage furrow progression (31). Since Y2H analyses can occasionally generate ambiguous results, we sought to corroborate these findings in an independent assay. To this end, we generated genetic knockout cell lines devoid of RacA and RacE in the AX2 wild type (WT) strain (Fig. 1B). Then, we monitored localization of constitutively active ForA fused to GFP in these knockouts. As shown in Fig. 1C, ForA was normally targeted to the cell cortex in *racA*<sup>-</sup> cells, but failed to localize to the cortex in *racE*<sup>-</sup> cells, strongly suggesting a physiological interaction between ForA and RacE. Consistently, the purified N-terminus of ForA also physically interacted with GMP-PNP-loaded RacE in pull-down experiments (Fig. 1D). In addition, constitutively active RacE was capable to release autoinhibition of an inactive formin sandwich complex formed by N- and C-terminal fragments of ForA in both pulldowns and pyrene assays (Fig. 1D and E). Finally, we monitored localization of active RacE fused to YFP in cells in 2D-confinement, i.e. under a thin sheet of agar. Unlike previous work that failed to detect active RacE in the cleavage furrow of unconfined cells (32), the active

341  
342  
343  
344  
345  
346  
347  
348  
349  
350  
351  
352  
353  
354  
355  
356  
357  
358  
359  
360  
361  
362  
363  
364  
365  
366  
367  
368  
369  
370  
371  
372  
373  
374  
375  
376  
377  
378  
379  
380  
381  
382  
383  
384  
385  
386  
387  
388  
389  
390  
391  
392  
393  
394  
395  
396  
397  
398  
399  
400  
401  
402  
403  
404  
405  
406  
407  
408



409  
410  
411  
412  
413  
414  
415  
416  
417  
418  
420  
421  
422  
423  
424  
425  
426  
427  
428  
429  
430  
431  
432  
433  
434  
435  
436  
437  
438  
439  
440  
441  
442  
443  
444  
445  
446  
447  
448  
449  
450  
451  
452  
453  
454  
455  
456  
457  
458  
459  
460  
461  
462  
463  
464  
465  
466  
467  
468  
469  
470  
471  
472  
473  
474  
475  
476

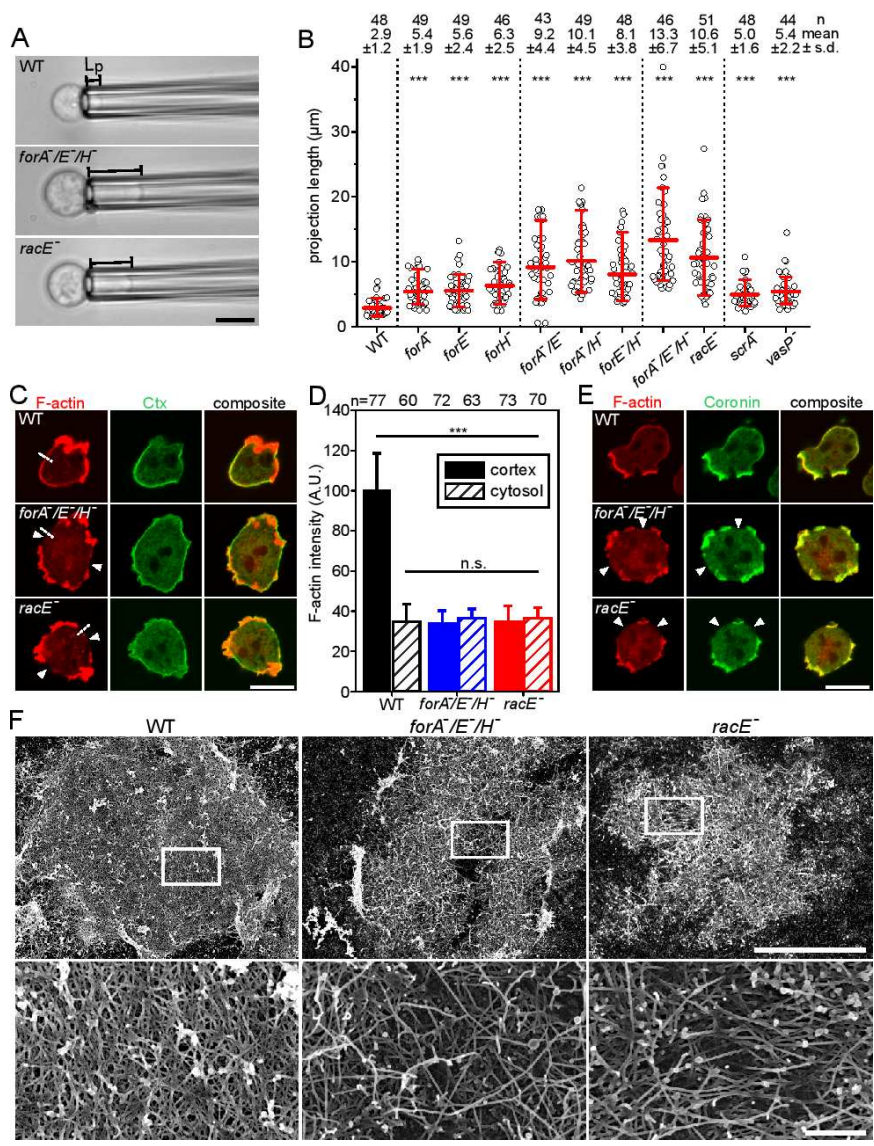


**Fig. 4.** Elimination of the three cortical formins or of RacE increasingly impairs cortical rigidity and disrupts the contractile actin cortex. (A) Projection length (Lp) of WT and the mutant cells indicated was determined by micropipette aspiration using a constant suction pressure of 500 Pa from time-lapse movies and correspond to Movie S2. Scale bar, 10 µm. (B) Quantitative analysis of the projection lengths of probed cells. n, number of analyzed cells, \*\*\*P < 0.001 by Mann-Whitney rank sum test. Statistical differences refer to WT. (C) Defects of the actin cortex in *forA/E/H* and *racE* mutants. Fixed WT and mutant cells were stained with a monoclonal Ctx antibody (green) to visualize PI(4,5)P2-containing membranes and F-actin with phalloidin (red). The white arrow heads indicate regions of low cortical density in the mutants. Scale bar, 10 µm. (D) Quantification of cortical and intracellular actin in WT and mutant cells. Average intensity profiles along 5 pixel wide lines as shown in (C) by the white dashed lines. n, number of analyzed cells; error bars, standard deviations (s.d). (E) Prominent cortical F-actin assemblies outside the breaches in *forA/E/H* and *racE* cells are identified as protrusions through containing coronin (green), particularly marking Arp2/3 complex-driven actin networks, and phalloidin-stained F-actin (red). Scale bar, 10 µm. (F) Representative SEM micrographs of detergent-extracted WT and mutant cells (low magnification and high magnification of insets shown at top and bottom, respectively). Scale bars, 5 µm (overview) and 0.5 µm (insets).

477  
478  
479  
480  
481  
482  
483  
484  
485  
486  
487  
488  
489  
490  
491  
492  
493  
494  
495  
496  
497  
498  
499  
500  
501  
502  
503  
504  
505  
506  
507  
508  
509  
510  
511  
512  
513  
514  
515  
516  
517  
518  
519  
520  
521  
522  
523  
524  
525  
526  
527  
528  
529  
530  
531  
532  
533  
534  
535  
536  
537  
538  
539  
540  
541  
542  
543  
544

GTPase accumulated about two-fold in the cleavage furrow as compared to pole regions upon 2D-confinement (Fig. 1F). Moreover, like active ForA, the GTPase was also markedly enriched in the rear cortex of migrating cells (Fig. 1G and ("SI Appendix, Movie S1")), substantiating the view that ForA is regulated by RacE.

**Active RacE additionally interacts with cortical formins ForE and ForH.** Based on the critical effect of RacE deficiency on cytokinesis, contractility and the regulation of ForA, and the fact that ForE constitutes the only known Rho-family GTPase in *Dictyostelium* with RhoA-like functions, we reasoned that additional formins may interact with the active GTPase and localize to the cell cortex to safeguard cortex functions. Thus, from the 10 formins expressed in *Dictyostelium* cells (33), we screened all four potential candidates expressed at the vegetative stage, referred to as ForB, ForE (dDia3), ForH (dDia2) and ForF (dDia1) with Rho- GTPases in the Y2H assay. ForI could be excluded from the screen because of lacking the regulatory GBD, and ForG was omitted due to its specific interaction with active Ras (23).. Strong and specific interactions with active RacE were identified for two of the four tested formins. ForE interacted with active variants of RacE and RacF2 (Fig. 2A). However, since RacF2 appears

to carry out specific functions in macrocyst formation during the sexual cycle (34), we did not follow that lead. Unexpectedly, active RacE also interacted with ForH (Fig. 2B), previously shown to operate in filopodia formation (35).

Next, we examined the subcellular localization of constitutively active ForE and ForH variants lacking the DAD regions and fused to YFP in freely moving or 2D-confined WT and *racE* cells. Consistent with previous work (35), ectopic expression of active ForH in WT cells triggered the formation of numerous filopodia, with the active formin being markedly enriched at the cell cortex and filopodial tips (Fig. 2C and ("SI Appendix, Fig. S3")). In 2D-confinement, filopodia formation was strongly suppressed and active ForH accumulated in the rear cortex of migrating cells, resembling localization of active ForA under the same conditions (17). To our surprise, and as opposed to the entirely diffuse localization of active ForA in *racE* cells, constitutively active ForH was still able to trigger filopodia formation and accumulate in the cell cortex of freely moving *racE* mutant cells. In 2D-confinement, however, the formin became largely cytosolic and failed to be incorporated into the rear.

Active ForE also markedly localized to the cortex of unconfined WT cells and to distal tips of filopodia (Fig. 2D and Fig.

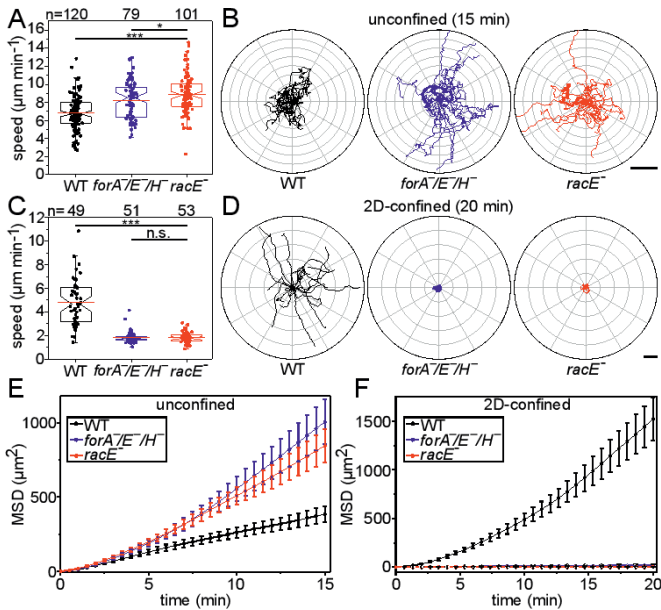


**Fig. 5.** *ForA/E/H* and *racE* mutants cannot migrate in 2D-confinement. (A and C) Box plots summarizing the random migration speed of WT, *ForA/E/H* and *racE* cells in (A) unconfined and (C) 2D-confinement conditions. At least three movies from three independent experiments were analyzed for each cell type. n, number of cells analyzed. n.s. non-significant, \* p<0.05, \*\*\* p<0.001 by Mann-Whitney rank sum test. (B and D) Radar plots showing the trajectories of 20 randomly migrating WT, *ForA/E/H* and *racE* cells in unconfined and 2D-confinement conditions as indicated. Note the high directional persistence of the mutant cells in unconfined settings. Scale bars, 30  $\mu\text{m}$  for (B) and 20  $\mu\text{m}$  for (D). (E and F) Analysis of the mean square displacement of WT, *ForA/E/H* and *racE* cells migrating in unconfined and 2D-confined conditions as indicated. Error bars represent s.e.m. n as in (A) and (C).

S3). In the *racE* mutant, however, the formin was not targeted to the cortex and remained diffuse in the cytoplasm under both experimental settings, implying a requirement for RacE signaling to mediate appropriate subcellular targeting. Consistently, and as previously shown for RacE (36), active ForA, ForH and ForE localized in folate gradients after treatment with latrunculin B specifically on that portion of the plasma membrane facing lower chemoattractant concentrations ("SI Appendix, Fig. S4"). Thus, *Dictyostelium* cells express three RacE-regulated formins that accumulate in cell cortex and rear of cells migrating in 2D-confinement.

**Elimination of the three cortical formins causes drastic cytokinesis and developmental defects.** To uncover a potential functional redundancy of these three RacE-regulated, cortical formins, we eliminated them all either alone or in combination by gene disruption, to obtain a complete collection of single- and double-mutants as well as a cell line lacking all three formins (Fig. 3A and ("SI Appendix, Fig. S5")). Mutant lines devoid of either ForA or ForH have previously been described (17, 35). Next, we asked whether, or to which extent, cytokinesis is impaired after consecutive elimination of these cortical formins. For that, we first assayed cytokinesis of the *forA*-single, the *forA/E*-double and the *forA/E/H*-triple mutant at high stringency in shaken suspension, and compared effects obtained with RacE- and myosin II-null mutants known to exhibit strong defects in mitotic cell division under these conditions (37, 38). After fixing the cells together with DAPI, we quantified number of nuclei per cell as an unambiguous readout for cytokinesis defects. In cells harvested from shaken suspension after 48 h, the vast majority of WT cells, *forA*-single, and *forA/E*-double mutants was mono- or bi-nucleated, although a few *forA/E*-double mutant cells also displayed three

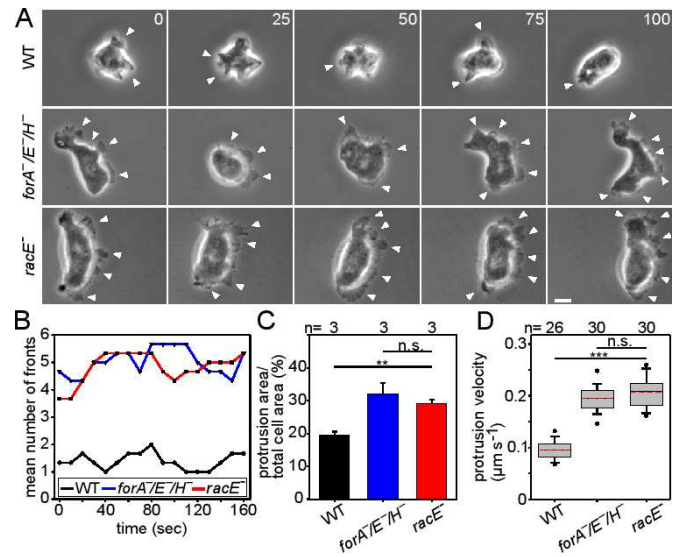


**Fig. 6.** *ForA/E/H* and *racE* mutants form multiple and faster protruding fronts. (A) Gallery with stills from a phase-contrast time-lapse series of randomly migrating WT and mutant cells in unconfined settings corresponding to Movie S4 shows the recurring formation of multiple fronts (white arrow heads) in *ForA/E/H* and *racE* mutants. Time is in seconds. Scale bar, 5  $\mu\text{m}$ . (B) Quantification of the average number of protruding fronts in migrating WT and mutant cells as shown in (A). (C) Quantification of the ratio of protrusion area over total cell area in WT and indicated mutant cells. Error bars represent s.e.m.. n.s. non-significant, \*\* p<0.01 by Mann-Whitney rank sum test. (D) Average protrusion velocities of fronts in WT and mutant cells. Boxes include 50% and whiskers 80% of all measurements, dots represent the 5<sup>th</sup>/95<sup>th</sup> percentile. n, number of cells analyzed. n.s. non-significant, \*\*\* p<0.001 by Mann-Whitney rank sum test.

or four nuclei (Fig. 3 B and C). By contrast, the *forA/E/H*-triple mutant exhibited a severe cytokinesis defect and was virtually indistinguishable from *racE* and *mhcA* mutants, since about 90% of these mutants developed highly multinucleated cells (Fig. 3 B and C). To exclude the possibility that a specific formin executes a predominant function in cytokinesis, we additionally performed these cytokinesis assays with all three combinations of double-mutant cells. Although mutant cell lines lacking ForH had a stronger tendency to form multinucleated cells, about 80% of all three formin double-null mutants still contained cells with only one or two nuclei ("SI Appendix, Fig. S6"). Thus, a severe cytokinesis defect was only manifested after inactivation of all three cortical formins.

Importantly, multicellular development also depends on contractility and cortical integrity. Myosin II mutants for instance cannot advance beyond the aggregation stage (39) and double mutants devoid of Ctx I/Ctx II known to tether cortical actin filaments to the membrane entirely fail to develop (40). Thus, we additionally compared multicellular development of WT cells, *forA*-single, *forA/E*-double, and the *forA/E/H*-triple mutant on bacterial lawns. Similar to WT, single- and double formin mutants were still able to advance through development and produce viable spores, although fruiting bodies of the *forA/E*-double mutant already appeared considerably smaller (Fig. 4D). Notably, the *forA/E/H*-triple mutant was completely blocked in development and not even able to aggregate. Thus, consistent with their overlapping functions in cytokinesis, all three formins have to be eliminated simultaneously to abrogate morphogenesis.

**ForA, ForE and ForH synergize in the maintenance of cortical integrity.** To quantify the assumed synergistic role of these formins in cortical integrity in the absence of adhesion forces, and to directly compare their contributions to this with those of *racE*, we performed micropipette aspiration assays (MPA)



681  
682  
683  
684  
685  
686  
687  
688  
689  
690  
691  
692  
693  
694  
695  
696  
697  
698  
699  
700  
701  
702  
703  
704  
705  
706  
707  
708  
709  
710  
711  
712  
713  
714  
715  
716  
717  
718  
719  
720  
721  
722  
723  
724  
725  
726  
727  
728  
729  
730  
731  
732  
733  
734  
735  
736  
737  
738  
739  
740  
741  
742  
743  
744  
745  
746  
747  
748

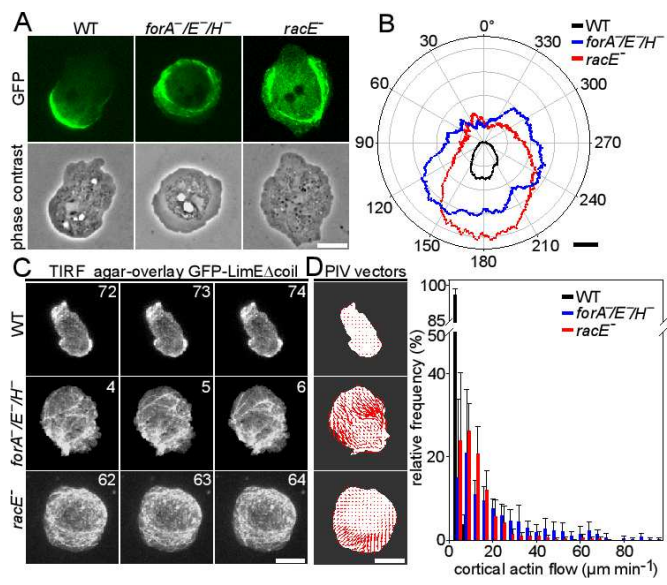


**Fig. 7.** *ForA/E/H* and *racE* mutants cannot polarize and exhibit a drastically increased cortical flow in 2D-confinement. (A) The characteristic localization of GFP-myosin II in the rear cortex of WT cells is abolished in *forA/E/H* and *racE* mutant cells illustrating a major defect in polarization. Still images from time-lapse movies correspond to Movie S6. Scale bar, 10  $\mu$ m. (B) Quantification of the width of the cortical myosin layer in WT and mutant cells determined by rotational analysis of the fluorescence signal from cells as shown in (A). Radar plot shows the mean myosin II band thickness of the cell lines indicated. Scale bar, 0.5  $\mu$ m. (C) Still images from TIRF time-lapse movies of WT and mutant cells expressing the F-actin probe GFP-LimE $\Delta$ coil in 2D-confined conditions under agar. Time is in seconds. Scale bar, 10  $\mu$ m. (D) PIV analyses of cortical actin flow in WT and mutant cells. Five consecutive frames recorded at 0.5 s intervals corresponding to Movie S7 were used for PIV analysis. The resulting vectors mark the mean actin velocity per frame (left). Distribution of actin flow velocities of the cell lines indicated reveal a strikingly increased actin flow in the mutants (right). Error bars are s.e.m..

of resuspended WT and mutant cells to measure their global mechanical resistance. To avoid secondary responses of the highly dynamic *Dictyostelium* cells to external suction pressure, we quantified the initial projection length ( $L_p$ ) of cells captured from suspension at a constant pressure of 500 Pa in MPA assays. Serial elimination of the formins correlated with increasing defects of cortical rigidity and peaked in the *forA/E/H*-triple mutant with an average indentation length of  $13 \pm 6.7 \mu$ m (mean $\pm$ s.d.) as opposed to  $3 \pm 1.2 \mu$ m in WT cells (Fig. 4 A and B). In contrast to many WT cells, *forA/E/H* cells were unable to withdraw from the micropipette even at this comparably low suction pressure, and all of them were ultimately sucked into the pipette within 5-10 min ("SI Appendix, Movie S2"). *RacE* cells also exhibited a major defect of cortical rigidity with an  $L_p$  of  $11 \pm 5.1 \mu$ m, although the defect was slightly weaker as compared to the formin triple-knockout mutant. Unexpectedly, however, and albeit none of the analyzed cells was able to completely withdraw from the pipette, almost all cells (98%) resisted complete aspiration at 500 Pa within 10 min. Finally, we also measured the cortical properties of mutant cells lacking the Arp2/3-complex activator Scar and the actin filament elongator VASP. Cortex rigidity of *scrA* and *vasP* cells was also clearly impaired as compared to control. However, the contribution of Scar and of VASP was moderate, since measured  $L_p$  values were only in the range of the formin single-knockout mutants. Thus, in *Dictyostelium* Arp2/3 complex and VASP appear to contribute far less to mechanical rigidity of the cortex as compared to formins.

Next, we examined the distribution of cortical F-actin in fixed WT, *forA/E/H* and *racE* cells after phalloidin staining. Additionally, we labelled the specimens for PI(4,5)P<sub>2</sub>-binding Ctx, to

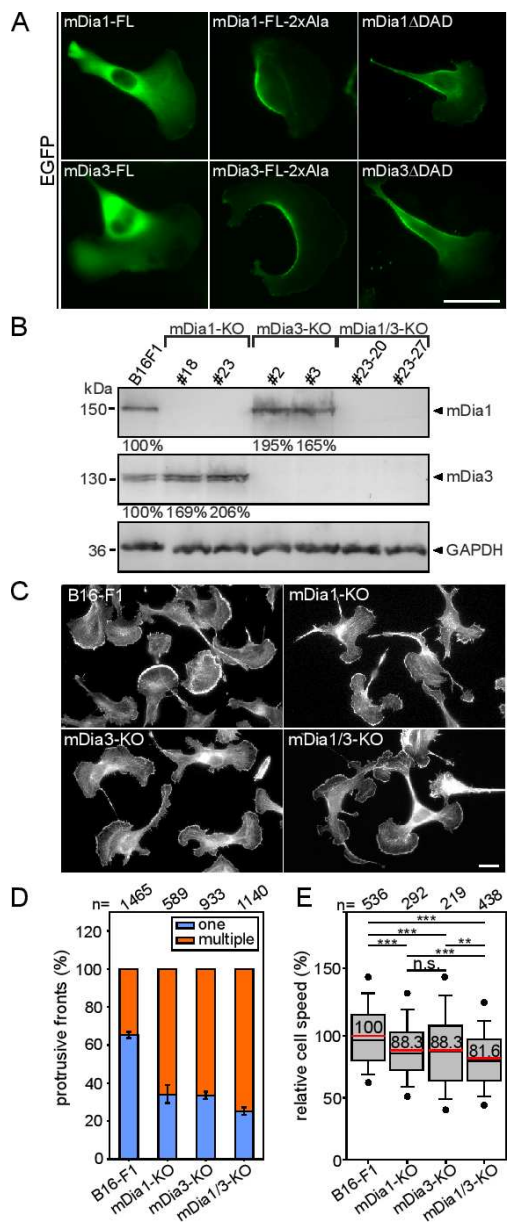


**Fig. 8.** Formation of multiple fronts and defects in polarization and migration in mDia1- and/or -3-deficient B16-F1 cells. (A) Subcellular localization of EGFP-mDia1 and -3 variants in B16-F1 cells migrating on laminin. While full-length (FL) mDia1 and -3 were cytosolic and largely excluded from protrusive fronts, constitutively active mDia1-FL-2xAla (M1182A and F1195A), mDia1 $\Delta$ DAD, mDia3-FL-2xAla (M1057A and F1170A) and mDia3 $\Delta$ DAD strongly accumulated in the rear cortex. Scale bar, 20  $\mu$ m. (B) Immunoblotting of individual and combined mDia1 and mDia3 KO clones as indicated, GAPDH: loading control. Numbers below respective lanes indicate relative changes of mDia1 and -3 expression levels normalized to GAPDH. (C) Polarization defects and formation of multiple fronts in respective cell types, as revealed by phalloidin-staining. Note increasingly pronounced multiple-front phenotypes in single versus double (mDia1/3) KO cells. Scale bar, 10  $\mu$ m. (D) Quantification of protrusive fronts (one versus multiple) from images as shown in C. Error bars, s.e.m. from at least six independent experiments, n, cell number. (E) Quantification of random migration of respective cell types on laminin. Boxes include 50% and whiskers 80% of all measurements, dots represent the 5th/95th percentile. n.s. non-significant, \*\* p<0.01, \*\*\* p<0.001 by Mann-Whitney rank sum test. n, number of tracked cells.

visualize the lipid gradient between front and rear in polarized *Dictyostelium* cells. In highly polarized WT cells, the bulk of F-actin was concentrated in the leading edge and contained only

749  
750  
751  
752  
753  
754  
755  
756  
757  
758  
759  
760  
761  
762  
763  
764  
765  
766  
767  
768  
769  
770  
771  
772  
773  
774  
775  
776  
777  
778  
779  
780  
781  
782  
783  
784  
785  
786  
787  
788  
789  
790  
791  
792  
793  
794  
795  
796  
797  
798  
799  
800  
801  
802  
803  
804  
805  
806  
807  
808  
809  
810  
811  
812  
813  
814  
815  
816

817 small amounts of Ctx, while the rear and lateral sides, encom- 885  
818 passing the thin layer of cortical actin, were strongly enriched 886  
819 for Ctx (Fig. 4C). By contrast, *forA*<sup>-</sup>/*E*<sup>-</sup>/*H*<sup>-</sup> and *racE*<sup>-</sup> mutants 887  
820 were rounder overall and did not show the characteristic Ctx 888  
821 differential. Most notably, large sections of the cortex in both 889  
822 mutants were devoid of the cortical actin layer, while remaining 890  
823 segments of the cortex still contained prominent F-actin assem- 891  
824 blies. Quantification of phalloidin fluorescence intensities across 892  
825 the cortex in actin-deficient areas confirmed this view (Fig. 4D), 893  
826 and was further substantiated by time-lapse imaging of WT and 894  
827 mutant cells expressing the F-actin probe LimEΔcoil-GFP ("SI 895  
828 Appendix, Movie S3"). We hypothesized that the thin layer that is 896  
829 missing in the mutants corresponds to the contractile actin cortex, 897  
830 whereas the remaining and prominent F-actin assemblies repre- 898  
831 sent Arp2/3 complex-driven F-actin structures such as leading 899  
832 edges or endocytic cups. Thus, we labelled WT and mutant cells 900  
833 with phalloidin and for the F-actin binding protein coronin, which 901  
834 is a central constituent of Arp2/3 complex-mediated F-actin net- 902  
835 works (41). Consistent with the key function of Arp2/3 complex 903  
836 in protrusion, coronin was strongly enriched in the leading edges 904  
837 of WT cells (Fig. 4E). Notably, coronin was depleted from actin- 905  
838 deficient regions, but co-localizing with the prominent F-actin 906  
839 assemblies in *forA*<sup>-</sup>/*E*<sup>-</sup>/*H*<sup>-</sup> and *racE*<sup>-</sup> mutants, strongly suggesting 907  
840 that these structures are nucleated by Arp2/3 complex. Finally, 908  
841 we explored the ultrastructural cortex architecture by scanning 909  
842 electron microscopy (SEM) after detergent extraction of cells. As 910  
843 opposed to the dense, cortical meshwork of WT cells with numer- 911  
844 ous overlapping filaments, elimination of the three formins or of 912  
845 RacE caused marked differences in cortical actin organization, 913  
846 including a lower filament density interspaced with large gaps 914  
847 containing much fewer filaments with different geometry (Fig. 915  
848 4F).

849 **Cortical formins are essential for motility in 2D-** 916  
850 **confinement.** Loss of ForA was previously shown to affect 917  
851 cell migration in unconfined and 2D-confined scenarios (17). 918  
852 Thus, we analyzed random cell migration of freely moving and 919  
853 2D-confined *forA*<sup>-</sup>/*E*<sup>-</sup>/*H*<sup>-</sup> and *racE*<sup>-</sup> mutants in phosphate buffer 920  
854 (PB) employing phase-contrast time-lapse microscopy, and 921  
855 compared migration rates of the mutants to that of WT cells. 922  
856 Additionally, we also determined mean square displacement 923  
857 (MSD) to discriminate locally restricted movement or wiggling of 924  
858 cells from effective directional cell migration (42). Intriguingly, 925  
859 elimination of ForA, ForE and ForH or of RacE even increased 926  
860 the speed of randomly migrating, mutant cells in unconfined 927  
861 environments to  $8.2 \pm 2.1 \mu\text{m}\cdot\text{min}^{-1}$  (*forA*<sup>-</sup>/*E*<sup>-</sup>/*H*<sup>-</sup>) or  $8.9 \pm 2.1$  928  
862  $\mu\text{m}\cdot\text{min}^{-1}$  (*racE*<sup>-</sup>) (mean $\pm$ s.d.) as compared to WT controls 929  
863 with  $6.8 \pm 1.8 \mu\text{m}\cdot\text{min}^{-1}$  (Fig. 5 A and B). However, when 930  
864 compressed under a sheet of agar, *forA*<sup>-</sup>/*E*<sup>-</sup>/*H*<sup>-</sup> and *racE*<sup>-</sup> mutants 931  
865 were abrogated for migration ( $1.9 \pm 0.59 \mu\text{m}\cdot\text{min}^{-1}$  and  $1.8 \pm$  932  
866  $0.4 \mu\text{m}\cdot\text{min}^{-1}$ ), as assessed by tracking of the centroids when 933  
867 compared to WT ( $4.8 \pm 1.9 \mu\text{m}\cdot\text{min}^{-1}$ ) (Fig. 5 C and D). 934  
868 Consistent with their higher motility in unconfined settings, a 935  
869 large proportion of both mutants cells were more directional 936  
870 and had higher MSD values as compared to control (Fig. 5 E). 937  
871 In marked contrast, the MSD values of both mutants virtually 938  
872 dropped to zero in 2D-confinement, illustrating their inability 939  
873 to migrate under agar, whereas WT cells were still able to 940  
874 efficiently migrate under these conditions (Fig. 5F). These 941  
875 findings substantiate the fundamental role of the contractile 942  
876 actin cortex for cell migration in confinement. 943

877 **Mutants lacking cortical formins or RacE form multiple** 944  
878 **fronts.** Amoeboid cells such as *Dictyostelium* cells generally 945  
879 exhibit only weak adhesion to the substrate to allow for fast mi- 946  
880 gration in unconfined settings. In *Dictyostelium* cells impaired in 947  
881 the cortical actin cytoskeleton, cell behavior or establishment and 948  
882 maintenance of cell shape are expected to be stronger affected by 949  
883 membrane tension. To test this hypothesis, we imaged freely mov- 950  
884 ing *forA*<sup>-</sup>/*E*<sup>-</sup>/*H*<sup>-</sup> and *racE*<sup>-</sup> mutants at high magnification by time- 951  
885 lapse phase contrast microscopy, and compared their activities to 952

885 ing *forA*<sup>-</sup>/*E*<sup>-</sup>/*H*<sup>-</sup> and *racE*<sup>-</sup> mutants at high magnification by time- 951  
886 lapse phase contrast microscopy, and compared their activities to 952  
887 those of WT cells. WT cells were more spherical and typically 953  
888 formed one or two protruding fronts in the form of pseudopods 954  
889 or macropinosomes at a given time. By contrast, *forA*<sup>-</sup>/*E*<sup>-</sup>/*H*<sup>-</sup> and 955  
890 *racE*<sup>-</sup> mutants were considerably flatter, as evidenced by strongly 956  
891 reduced halos in phase-contrast images at their cell boundaries. 957  
892 Notably, about 33% of *forA*<sup>-</sup>/*E*<sup>-</sup>/*H*<sup>-</sup> cells and 19% of *racE*<sup>-</sup> cells in- 958  
893 termittently exhibited a fan-shaped, keratocyte-like morphology 959  
894 and migrated with high, directional persistence, which was con- 960  
895 trasted by only 6% of highly directional WT cells ("SI Appendix, 961  
896 Movie S4"). Remarkably, both mutants often developed multiple 962  
897 fronts exhibiting 5 or 6 lamellipodia-like pseudopods (Fig. 6 A 963  
898 and B and ("SI Appendix, Movie S5"). The elimination of formins 964  
899 and of RacE also substantially increased the combined protrusion 965  
900 area relative to total cell area in the mutants by more than 30% 966  
901 to  $32.0 \pm 5.7\%$  (*forA*<sup>-</sup>/*E*<sup>-</sup>/*H*<sup>-</sup>) and  $29.2 \pm 2.0\%$  (*racE*<sup>-</sup>) as compared 967  
902 to WT control ( $19.6 \pm 1.7\%$ , Fig. 6C). Moreover, the protrusion 968  
903 speed of the fronts in the mutants was about doubled to  $0.19 \pm$  969  
904  $0.03 \mu\text{m}\cdot\text{sec}^{-1}$  (*forA*<sup>-</sup>/*E*<sup>-</sup>/*H*<sup>-</sup>) and  $0.20 \pm 0.03 \mu\text{m}\cdot\text{sec}^{-1}$  (*racE*<sup>-</sup>) when 970  
905 compared to WT control ( $0.10 \pm 0.02 \mu\text{m}\cdot\text{sec}^{-1}$ ) (Fig. 6D). Inter- 971  
906 estingly, inhibition of myosin II by blebbistatin had little effect on 972  
907 the motility of *ForA*<sup>-</sup>/*E*<sup>-</sup>/*H*<sup>-</sup> and *racE*<sup>-</sup> mutant cells ("SI Appendix, 973  
908 Fig. S7"), excluding augmented actomyosin contractility as direct 974  
909 cause for these effects. Although RICM analyses revealed a larger 975  
910 contact area of mutant cells ("SI Appendix, Fig. S8 A and B"), 976  
911 they formed fewer actin foci, and these adhesion points were 977  
912 significantly shorter lived than those in controls ("SI Appendix, 978  
913 Fig. S8 C-E"). In line with these observations, the contact area 979  
914 of multiple front- or keratocyte-shaped cells was inhomogeneous 980  
915 and interspersed with less adhesive sections, as evidenced by 981  
916 RICM ("SI Appendix, Movies S6 and S7"). Thus, the combination 982  
917 of increased protrusive activity and decreased adhesiveness in the 983  
918 mutants may explain the highly directional persistence in motility 984  
919 assays. Finally, we noticed that the growth of initially formed 985  
920 fronts in the mutants typically ceased when multiple, competing 986  
921 protrusions were formed on the opposite side of the cell. In these 987  
922 cases, initial fronts rapidly lost adhesion to the underlying surface 988  
923 and were effectively retracted into the cell body ("SI Appendix, 989  
924 Fig. S9 and Movies S 6 and S8"). 990

925 **Polarity defects and dramatically increased cortical actin** 991  
926 **flow in *forA*<sup>-</sup>/*E*<sup>-</sup>/*H*<sup>-</sup> and *racE*<sup>-</sup> mutants.** An intact contractile 992  
927 actin cortex of amoeboid cells regulates cell migration in 2D- 993  
928 confinement by guiding hydrostatic pressure, created by acto- 994  
929 myosin contraction in the rear, to the front to promote leading 995  
930 edge protrusion (17). Thus, we monitored myosin II and F-actin 996  
931 representing the two main components of the contractile machin- 997  
932 ery in WT and mutant cells after mechanical stress in confinement 998  
933 under agar. WT cells expressing fluorescently-tagged heavy chain 999  
934 of myosin II were highly polarized, and the motor protein was 1000  
935 continuously concentrated in a compact, crescent-like sheet at 1001  
936 the rear cortex beneath the plasma membrane (Fig. 7A and 1002  
937 ("SI Appendix, Movie S9"). In striking contrast, *forA*<sup>-</sup>/*E*<sup>-</sup>/*H*<sup>-</sup> and 1003  
938 *racE*<sup>-</sup> mutants remained highly unpolarized in 2D-confinement, 1004  
939 as evidenced by the aberrant circular localization of myosin II in 1005  
940 a band-like fashion along most of the cell periphery, albeit this 1006  
941 phenotype was slightly less prominent in *racE*<sup>-</sup> cells (Fig. 7A). 1007  
942 Moreover, myosin II did not accumulate in a crisp band as in 1008  
943 WT cells, but was dispersed into multiple, string-like assemblies 1009  
944 in the mutants. Myosin II was also largely dislodged from the 1010  
945 membrane and was instead strongly enriched at an endoplasm- 1011  
946 ectoplasm interface separating the organelle free area from the 1012  
947 cell interior (Fig. 7A). Consistently, time-lapse imaging of the 1013  
948 mutant cells revealed a highly erratic behavior of myosin II as- 1014  
949 sociated with intense blebbing, substantiating the massive defects 1015  
950 in the contractile cell cortex of mutant cells ("SI Appendix, Movie 1016  
951 S9"). Quantification of myosin II band width as well as its radial 1017  
952



distribution in WT and mutant cells in polarity plots corroborated this view (Fig. 7B).

We then analyzed the dynamic behavior of cortical actin filaments at the ventral plasma membrane by total internal reflection fluorescence (TIRF) microscopy in WT and mutant cells after confinement under agar. In WT cells, cortical actin, visualized by the F-actin marker LimEΔcoil-GFP, was organized into a delicate, filamentous web, interspaced with dynamic actin foci, which accumulated most strongly in protruding fronts evidently driven by Arp2/3 complex-mediated actin assembly (Fig. 7C and ("SI Appendix, Movie S10")). A filamentous network was also observed in the *forA*<sup>-</sup>/*E*<sup>-</sup>/*H*<sup>-</sup> and *racE*<sup>-</sup> mutants. However, presumably due to the high membrane tension and their strong polarization defect in 2D-confinement, they did not form protruding fronts. Moreover, as assessed from TIRF time-lapse imaging, the dynamics of cortical actin filaments was drastically changed as compared to control. These filaments were rapidly pulled into the cell center in a process reminiscent of actin retrograde flow in higher eukaryotes. Particle image velocimetry (PIV)-based quantification of cortical actin flow confirmed this notion (Fig. 7D). The velocity distribution showed flows of up to 72 μm·min<sup>-1</sup> in *racE*<sup>-</sup> cells and almost up to 100 μm·min<sup>-1</sup> in the *forA*<sup>-</sup>/*E*<sup>-</sup>/*H*<sup>-</sup> mutant as compared to the average flow with 1.48±1.08 μm·min<sup>-1</sup> (mean±s.d.) in WT cells (Fig. 7E). Consistently, PIV analyses further revealed that the region with fastest actin filament flows overlap with myosin II-enriched regions in *forA*<sup>-</sup>/*E*<sup>-</sup>/*H*<sup>-</sup> and *racE*<sup>-</sup> mutants (Fig. 7A and E and ("SI Appendix, Fig. S10")). Together, these data strongly suggest that filaments nucleated by cortical formins regulate subcellular myosin II localization and cortical actin flow under mechanical stress.

**Cell lines lacking murine mDia1 and -3 display phenotypes indicative of conserved, cortical functions.** To explore whether our observations are generalizable to higher eukaryotes, we analyzed mammalian formins in highly motile B16-F1 mouse melanoma cells. Since mDia subfamily formins (1, 2, and 3) are regulated by RhoA (43), which is well established to drive contractility, we focused on subcellular localization of EGFP-tagged mDia variants after ectopic expression in B16-F1 cells. Consistent with our previous findings (17), we found constitutively active mDia1 variants, i.e. mDia1<sup>ΔDAD</sup> as well as the newly designed point mutant mDia1-FL-2xAla (M1182A and F1195A), which is expected to release autoinhibition of the FL protein (44), to localize prominently in the cell rear, whereas the full length, autoinhibited protein remained cytosolic (Fig. 8A). Virtually identical results were obtained with corresponding mDia3 variants (Fig. 8A), whereas active mDia2 was not found in the cell rear, but mostly targeted to filopodia tips (45). To evaluate mDia functions in the mammalian cell cortex, we employed CRISPR/Cas9-mediated disruption of the genes encoding mDia1 and -3, both individually and in combination in B16-F1 cells. Loss of respective protein in independent, clonal cell lines was confirmed by immunoblotting (Fig. 8B). Interestingly, mDia1 levels were evidently increased in both mDia3-KO cell lines, and *vice versa*, indicative of compensatory, regulatory mechanisms presumably serving to sustain sufficient levels of these cortical polarization (Fig. 8B). Phalloidin stainings revealed defects in cell polarization as well as markedly increased frequencies in mDia1 and -3 single mutants of cells forming multiple fronts, a phenotype that was even further increased in mDia1/3 double-KO cells (Fig. 8C and D) and strikingly reminiscent of cortical formin pathway KOs in *Dictyostelium*. Next, we analyzed random cell migration of B16-F1 wildtype and mutant cells on laminin using time-lapse, phase-contrast microscopy. Interestingly, as opposed to *Dictyostelium* cells migrating without 2D-confinement, cell depolarization and apparent stimulation of the multiple front phenotype reduced the efficiency of the highly adhesive mode of melanoma cell migration, likely caused by inefficient protrusion

in a productive, migratory direction. Specifically, whereas single mDia1 and -3 mutants displayed a moderate, but statistically significant reduction of migration rate in this assay (by 11.7%), removal of both mDia1 and -3 decreased migration even further (by 18.4%; Fig. 8E). Together, these data strongly suggest the RhoA-effectors of the mDia formin subfamily, in particular mDia1 and -3 to exert functions in the actin cortex that are conserved in evolution from *Dictyostelium* to mammals.

## Discussion

Over thirty years ago, Bray and White postulated that cortical contractility may not only contribute to retraction of the trailing edge, but also to ingression of the cleavage furrow during cytokinesis (46). Since then, localization and participation in both processes has been demonstrated for numerous cell cortex components including myosin II (47), Ctx (27), PTEN (48) and IQGAP family members (28). Here, we demonstrated that three DRFs, ForA, ForE and ForH act synergistically in the assembly of actin filaments in the contractile actin cortex as evidenced by the increasing severity of additive KO phenotypes, which directly correlated with a gradual decrease in mechanical cortex rigidity. We also showed that the active form of the Rho family GTPase RacE, binds to the GBD of ForA, releasing its autoinhibition to initiate actin assembly. RacE shows considerable sequence similarity with Rho proteins from other species and represents the closest homologue of mammalian RhoA in *Dictyostelium* (36, 49). The phenotype of *racE*<sup>-</sup> cells was similar to that of the triple knockout DRF cells, including large cytokinesis defects in suspension (31) as well as large effects on development (36). This reinforces the idea that the DRFs are required for filament formation, and this is regulated by RacE. Moreover, RacE localizes to the cell rear as well as cleavage furrow in mitotic cells, and is essential for cortical localization of ForA and ForE.

Similar to the redundancy in cortical actin organization exhibited by DRFs in *Dictyostelium*, we also found stronger, complementary phenotypes after combined inactivation of the formins mDia1 and -3 in B16-F1 mouse melanoma cells. This redundancy of the microfilament system is a common phenomenon for essential cellular activities, and has been observed previously for the actin-crosslinking proteins α-actinin and filamin (50) and for Ctx I and II (51) in *Dictyostelium*. While ForA, ForE and ForH act synergistically in actin filament assembly in the contractile actin cortex, it is likely that they also have isoform specific roles and can be activated by other signaling pathways. For example, we found that constitutively active ForH localized to the cortex in unconfined *racE*<sup>-</sup> cells, but remained largely cytosolic after compression in 2D-confinement, suggesting multiple interactors mediate its subcellular targeting. Of these, RacE is presumably important for ForH targeting under mechanical stress. Incidentally, ForH was recently also found as potential RacE interactor by mass spectrometry (52). In addition, active ForH and ForE also trigger filopodia formation, but as both cortex and filopodia constitute F-actin structures directly associated with the plasma membrane, these actin assembly factors may well participate in the formation of various membrane-associated structures entailing long, unbranched filaments.

The strong effects on cytokinesis and cortex-dependent functions in *forA*<sup>-</sup>/*E*<sup>-</sup>/*H*<sup>-</sup> are similar to those found in *racE*<sup>-</sup> cells. This indicates the phenotypic effect of *racE* gene elimination to derive from the lack of *forA/E/H* activation. Consistent with this, none of wild type formins (ForA, ForE or ForH) localized to the cortex as they are likely autoinhibited ("SI Appendix, Fig. S11") and (17). We also found that active RacE accumulates in the cleavage furrow of mitotic cells upon 2D-confinement, implying that it plays a role in regulating cytokinesis by recruitment and activation of cortical formins at this site.

Both *forA*<sup>-</sup>/*E*<sup>-</sup>/*H*<sup>-</sup> and *racE*<sup>-</sup> mutants displayed flat morphologies and formation of multiple, dynamic multi-directional protrusions along the cell contour. In agreement with recent work analyzing enhanced expansion of lamellipodial networks upon reduction of plasma membrane load (2), and considering theoretical calculations of cortex mechanics (53), these data imply that cells harboring a compromised viscoelastic cell cortex may experience reduced resistance to actin polymerization forces in protrusions. If correct, this could well cause the formation of amplified protrusions and multiple fronts observed in our mutants. Multiple protrusion formation in *Dictyostelium* was accompanied by adhesion weakening and irregular detachment. Consequently, most unconfined *forA*<sup>-</sup>/*E*<sup>-</sup>/*H*<sup>-</sup> and *racE*<sup>-</sup> cells, in some instances resembling fan-shaped keratocytes, migrated faster and more directional than their wildtype controls. These phenotypes appeared at the expense of the more amoeboid type of migration usually seen in *Dictyostelium*.

Of note, the inhibition of myosin II by blebbistatin had little effect on the motility of keratocytes (54) as well as *ForA*<sup>-</sup>/*E*<sup>-</sup>/*H*<sup>-</sup> and *racE*<sup>-</sup> mutant cells ("SI Appendix, Fig. S7"). This indicates that the migratory modes adopted by these cell types and/or experimental conditions are less dependent on cortical contractility than during amoeboid or canonical, mesenchymal migration, and additionally mostly driven by the amplified network expansion activity at the leading edges of these cells (55). Interestingly, the migratory behavior of *Dictyostelium* cells can be switched from amoeboid to keratocyte-like by either decreasing PIP2 levels or increasing Ras/Rap signaling (56). Whether or not these phenotypes could relate to the molecular mechanisms described here will be an exciting topic of future study.

In 2-D confinement, *forA*<sup>-</sup>/*E*<sup>-</sup>/*H*<sup>-</sup> and *racE*<sup>-</sup> mutants are unable to localize myosin II properly to the cell cortex, polarize and migrate. Symmetry breaking obtained by an anisotropic distribution of components including myosin II drives both, rear retraction in directed cell migration and cytokinesis. How myosin II is localized to the cell cortex is still not fully understood, but has been proposed to include signaling and mechanical cues including myosin phosphorylation by MHCK-A, PTEN, Ctx I or talin in *Dictyostelium* (14, 48, 57, 58) or preferential binding to stretched actin filaments (59). In any case, a severely perturbed cortical actin cytoskeleton will likely interfere with myosin II positioning and activity through all these pathways. Our findings thus establish cortical formins as key to the establishment of polarity and properly regulated migration in both *Dictyostelium* and mammalian cells.

Consistent with the elimination of these formins or their activator RacE, SEM and live-cell TIRF imaging revealed cortical filament density in *forA*<sup>-</sup>/*E*<sup>-</sup>/*H*<sup>-</sup> and *racE*<sup>-</sup> cells to be reduced compared to WT, but raised the question as to which assembly factors are involved in generating the remaining cortical actin filaments. Our immunofluorescence results with fixed cells indicated these filaments to be primarily nucleated by remaining prominent actin assembly factors, such as Arp2/3 complex and VASP, although we cannot exclude at this stage the presence of

filaments assembled by other formins, for instance ForG, known to cooperate with Arp2/3 complex in large scale endocytosis (23) or of ForF (dDia1), which homogeneously accumulates in the entire pseudopod (60).

In 2-D confinement, *forA*<sup>-</sup>/*E*<sup>-</sup>/*H*<sup>-</sup> and *racE*<sup>-</sup> mutants exhibited exceptionally fast centripetal flows of residual cortical filaments at velocities of 50-100  $\mu\text{m}/\text{min}$ , which were contrasted by almost immobile cortical networks relative to the advancement of migrating, wildtype cells. This suggests that in 2D-confinement, *Dictyostelium* does not primarily use retrograde actin fluxes to drive force transmission during migration, as recently proposed for other cell types utilizing amoeboid motility (61, 62). However, the precise cause of the excessive cortical actin flows observed in the mutants remains to be clarified. An intact cortical cytoskeleton harbors various transmembrane proteins and receptors, potentially acting as barriers constraining lateral diffusion (63). Thus, we speculate that the increased cortical flows observed in our mutants are caused by diminished viscosities of their perturbed cortical networks.

Our initial characterization of genome-edited B16-F1 mouse melanoma mutants devoid of mDia1, mDia3 or both formins revealed striking similarities to the *Dictyostelium* system. Comparable to *Dictyostelium* ForA, ForE and ForH, both mammalian formins are regulated by Rho-subfamily proteins, which are ultimately linked to contractility. Active variants of mDia1 and -3, but not the autoinhibited full-length proteins localized prominently to the rear cortex in polarized B16-F1 cells, and the individual elimination of these formins triggered the formation of multiple protrusive fronts as well as substantial defects in polarization and migration. The fact that the phenotypes were noticeably amplified in double mutants reinforced the conclusion of their overlapping functions. This is consistent with a very recent study analyzing the contractile actin cortex in Sertoli cells of mouse seminiferous tubules (64). Loss of mDia1 and -3 in these cells compromised the cortical actin cytoskeleton leading to less dense F-actin meshworks ultimately resulting in impaired spermatogenesis. Taken together, our results suggest that formins are important in cell cortex establishment and maintenance, and that these functions are evolutionarily conserved across far distant organisms.

## Materials and Methods

A complete description of the methods is provided in SI Materials and Methods. This description includes construct generation, cell culture, transfections and establishment of *Dictyostelium* and B16-F1 mutants, protein purification, actin-assembly and pull-down assays, antibodies and immunoblots, imaging, aspiration assays, analyses of cell migration, Y2H assays, and quantification of actin flows and statistical analyses.

## Acknowledgements

We thank Annette Breskott for technical assistance and all members of the group for inspiring discussions. We further thank Martin Fuller for help with critical point drying and Stuart Micklethwaite and John Harrington of LEMAS (Leeds Electron Microscopy and Spectroscopy Centre) for help with collecting SEM images. This work was supported by Wellcome Trust to M.P. (094231/Z/10/Z), intramural funding from the Helmholtz Society to R.M. and K.R., and the Deutsche Forschungsgemeinschaft to K.R. (GRK2223/1) and J.F. (FA 330/12-1).

1. Blanchoin L, Boujemaa-Paterski R, Sykes C, Plastino J (2014) Actin dynamics, architecture, and mechanics in cell motility. *Physiol Rev* 94(1):235–63.
2. Mueller J, et al. (2017) Load Adaptation of Lamellipodial Actin Networks. *Cell* 171(1):188–200.e16.
3. Kage F, et al. (2017) FMNL formins boost lamellipodial force generation. *Nat Commun* 8. doi:10.1038/ncomms14832.
4. Sackmann E (2015) How actin/myosin crosstalks guide the adhesion, locomotion and polarization of cells. *Biochim Biophys Acta* 1853(11 Pt B):3132–42.
5. Paluch EK, Aspalter IM, Sixt M (2016) Focal Adhesion-Independent Cell Migration. *Annu Rev Cell Dev Biol* 32(1):469–490.
6. Bear JE, Haugh JM (2014) Directed migration of mesenchymal cells: where signaling and the cytoskeleton meet. *Curr Opin Cell Biol* 30:74–82.
7. Charras GT, Coughlin M, Mitchison TJ, Mahadevan L (2008) Life and Times of a Cellular Bleb. *Biophys J* 94(5):1836–1853.
8. Yoshida K, Soldati T (2006) Dissection of amoeboid movement into two mechanically distinct

modes. *J Cell Sci* 119(18):3833–3844.

9. Clark AG, Wartlick O, Salbreux G, Paluch EK (2014) Stresses at the cell surface during animal cell morphogenesis. *Curr Biol* 24(10):R484–94.
10. Chugh P, et al. (2017) Actin cortex architecture regulates cell surface tension. *Nat Cell Biol* 19(6):689–697.
11. Fehon RG, McClatchey AI, Bretscher A (2010) Organizing the cell cortex: the role of ERM proteins. *Nat Rev Mol Cell Biol* 11(4):276–287.
12. Maniti O, et al. (2012) Binding of moesin and ezrin to membranes containing phosphatidylinositol (4,5) biphosphate: A comparative study of the affinity constants and conformational changes. *Biochim Biophys Acta - Biomembr* 1818(11):2839–2849.
13. Stock A, et al. (1999) Domain analysis of cortaxillin I: Actin-bundling, PIP2-binding and the rescue of cytokinesis. *EMBO J* 18(19). doi:10.1093/emboj/18.19.5274.
14. Ren Y, et al. (2009) Mechanosensing through Cooperative Interactions between Myosin II and the Actin Crosslinker Cortaxillin I. *Curr Biol* 19(17):1421–1428.
15. Kee Y-S, et al. (2012) A mechanosensory system governs myosin II accumulation in dividing

- 1225 cells. *Mol Biol Cell* 23(8):1510–23.
- 1226 16. Salbreux G, Charras G, Paluch E (2012) Actin cortex mechanics and cellular morphogenesis. *Trends Cell Biol* 22(10):536–545.
- 1227 17. Ramalingam N, et al. (2015) A resilient formin-derived cortical actin meshwork in the rear drives actomyosin-based motility in 2D confinement. *Nat Commun* 6. doi:10.1038/ncomms9-496.
- 1228 18. Rottner K, Faix J, Bogdan S, Linder S, Kerkhoff E (2017) Actin assembly mechanisms at a glance. *J Cell Sci* 130(20). doi:10.1242/jcs.206433.
- 1229 19. Pollard TD (2007) Regulation of Actin Filament Assembly by Arp2/3 Complex and Formins. *Annu Rev Biophys Biomol Struct* 36(1):451–477.
- 1230 20. Kühn S, Geyer M (2014) Formins as effector proteins of Rho GTPases. *Small GTPases* 5(3):e983876.
- 1231 21. Lammers M, Rose R, Scrima A, Wittinghofer A (2005) The regulation of mDia1 by autoinhibition and its release by Rho\*GTP. *EMBO J* 24(23):4176–87.
- 1232 22. Li F, Higgs HN (2005) Dissecting Requirements for Auto-inhibition of Actin Nucleation by the Formin, mDia1. *J Biol Chem* 280(8):6986–6992.
- 1233 23. Junemann A, et al. (2016) A Diaphanous-related formin links Ras signaling directly to actin assembly in macropinocytosis and phagocytosis. *Proc Natl Acad Sci* 113(47):E7464–E7473.
- 1234 24. Bovellan M, et al. (2014) Cellular Control of Cortical Actin Nucleation. *Curr Biol* 24(14):1628–1635.
- 1235 25. Fritzsche M, Erlenkämper C, Moeendarbary E, Charras G, Kruse K (2016) Actin kinetics shapes cortical network structure and mechanics. *Sci Adv* 2(4):e1501337.
- 1236 26. Fukui Y, Inoué S (1991) Cell division in *Dictyostelium* with special emphasis on actomyosin organization in cytokinesis. *Cell Motil Cytoskeleton* 18(1):41–54.
- 1237 27. Weber I, et al. (1999) Cytokinesis mediated through the recruitment of cortexillins into the cleavage furrow. *EMBO J* 18(3):586–594.
- 1238 28. Faix J, et al. (2001) Recruitment of cortexillin into the cleavage furrow is controlled by Rac1 and IQGAP-related proteins. *EMBO J* 20(14):3705–15.
- 1239 29. Bohnert KA, Willet AH, Kovar DR, Gould KL (2013) Formin-based control of the actin cytoskeleton during cytokinesis. *Biochem Soc Trans* 41(6). Available at: <http://www.biochemsoctrans.org/content/41/6/1750.long> [Accessed May 25, 2018].
- 1240 30. Rivero F, Dislich H, Glöckner G, Noegel AA (2001) The Dictyostelium discoideum family of Rho-related proteins. *Nucleic Acids Res* 29(5):1068–79.
- 1241 31. Gerald N, Dai J, Ting-Beall HP, De Lozanne A (1998) A role for Dictyostelium racE in cortical tension and cleavage furrow progression. *J Cell Biol* 141(2):483–92.
- 1242 32. Laroche DA, Vithalani KK, De Lozanne A (1997) Role of Dictyostelium racE in cytokinesis: mutational analysis and localization studies by use of green fluorescent protein. *Mol Biol Cell* 8(5):935–44.
- 1243 33. Rivero F, et al. (2005) A comparative sequence analysis reveals a common GBD/FH3-FH1-FH2-DAD architecture in formins from Dictyostelium, fungi and metazoa. *BMC Genomics* 6(1):28.
- 1244 34. Muramoto T, Urushihara H (2006) Small GTPase RacF2 affects sexual cell fusion and asexual development in Dictyostelium discoideum through the regulation of cell adhesion. *Dev Growth Differ* 48(3):199–208.
- 1245 35. Schirenbeck A, Bretschneider T, Arasada R, Schleicher M, Faix J (2005) The Diaphanous-related formin dDia2 is required for the formation and maintenance of filopodia. *Nat Cell Biol* 7(6). doi:10.1038/ncb1266.
- 1246 36. Wang Y, Senoo H, Sesaki H, Iijima M (2013) Rho GTPases orient directional sensing in chemotaxis. *Proc Natl Acad Sci* 110(49):E4723–E4732.
- 1247 37. Chen P, Ostrow BD, Tafuri SR, Chisholm RL (1994) Targeted disruption of the Dictyostelium RMLC gene produces cells defective in cytokinesis and development. *J Cell Biol* 127(6). Available at: <http://jcb.rupress.org/content/127/6/1933.long> [Accessed May 25, 2018].
- 1248 38. Laroche DA, Vithalani KK, De Lozanne A (1996) A novel member of the rho family of small GTP-binding proteins is specifically required for cytokinesis. *J Cell Biol* 133(6):1321–9.
- 1249 39. Springer ML, Patterson B, Spudich JA (1994) Stage-specific requirement for myosin II during Dictyostelium development. *Development* 120(9):2651–60.
- 1250 40. Shu S, Liu X, Kriebel PW, Daniels MP, Korn ED (2012) Actin cross-linking proteins cortexillin I and II are required for cAMP signaling during Dictyostelium chemotaxis and development. *Mol Biol Cell* 23(2):390–400.
- 1251 41. Bretschneider T, et al. (2002) Dynamic organization of the actin system in the motile cells of Dictyostelium. *J Muscle Res Cell Motil* 23(7–8):639–49.
- 1252 42. Litschko C, et al. (2017) Differential functions of WAVE regulatory complex subunits in the regulation of actin-driven processes. *Eur J Cell Biol*. doi:10.1016/j.ejcb.2017.08.003.
- 1253 43. Lammers M, Meyer S, Kühlmann D, Wittinghofer A (2008) Specificity of Interactions between mDia Isoforms and Rho Proteins. *J Biol Chem* 283(50):35236–35246.
- 1254 44. Lammers M, Rose R, Scrima A, Wittinghofer A (2005) The regulation of mDia1 by autoinhibition and its release by Rho\*GTP. *EMBO J* 24(23):4176–4187.
- 1255 45. Block J, et al. (2008) Filopodia formation induced by active mDia2/Drf3. *J Microsc* 231(3). doi:10.1111/j.1365-2818.2008.02063.x.
- 1256 46. Bray D, White JG (1988) Cortical flow in animal cells. *Science* 239(4842):883–8.
- 1257 47. Moores SL, Sabry JH, Spudich JA (1996) Myosin dynamics in live Dictyostelium cells. *Proc Natl Acad Sci U S A* 93(1):443–6.
- 1258 48. Pramanik MK, Iijima M, Iwadate Y, Yumura S (2009) PTEN is a mechanosensing signal transducer for myosin II localization in Dictyostelium cells. *Genes Cells* 14(7):821–34.
- 1259 49. Vlahou G, Rivero F (2006) Rho GTPase signaling in Dictyostelium discoideum: Insights from the genome. *Eur J Cell Biol* 85(9–10):947–959.
- 1260 50. Witke W, Schleicher M, Noegel AA (1992) Redundancy in the microfilament system: abnormal development of Dictyostelium cells lacking two F-actin cross-linking proteins. *Cell* 68(1):53–62.
- 1261 51. Faix J, et al. (1996) Cortexillins, major determinants of cell shape and size, are actin-bundling proteins with a parallel coiled-coil tail. *Cell* 86(4). doi:10.1016/S0092-8674(00)80136-1.
- 1262 52. Senoo H, Cai H, Wang Y, Sesaki H, Iijima M (2016) The novel RacE-binding protein GflB sharpens Ras activity at the leading edge of migrating cells. *Mol Biol Cell* 27(10):1596–605.
- 1263 53. Sens P, Plastino J (2015) Membrane tension and cytoskeleton organization in cell motility. *J Phys Condens Matter* 27(27):273103.
- 1264 54. Keren K, Yam PT, Kinkhabwala A, Mogilner A, Theriot JA (2009) Intracellular fluid flow in rapidly moving cells. *Nat Cell Biol* 11(10):1219–1224.
- 1265 55. Keren K (2011) Cell motility: the integrating role of the plasma membrane. *Eur Biophys J* 40(9):1013–1027.
- 1266 56. Miao Y, et al. (2017) Altering the threshold of an excitable signal transduction network changes cell migratory modes. *Nat Cell Biol* 19(4):329–340.
- 1267 57. Steimle PA, et al. (2001) Recruitment of a myosin heavy chain kinase to actin-rich protrusions in Dictyostelium. *Curr Biol* 11(9):708–13.
- 1268 58. Tsuboi M, et al. (2012) Talin couples the actomyosin cortex to the plasma membrane during rear retraction and cytokinesis. *Proc Natl Acad Sci U S A* 109(32):12992–7.
- 1269 59. Uyeda TQP, Iwadate Y, Umeki N, Nagasaki A, Yumura S (2011) Stretching actin filaments within cells enhances their affinity for the myosin II motor domain. *PLoS One* 6(10):e26200.
- 1270 60. Winterhoff M, et al. (2014) The Diaphanous-related formin dDia1 is required for highly directional phototaxis and formation of properly sized fruiting bodies in Dictyostelium. *Eur J Cell Biol* 93(5–6). doi:10.1016/j.ejcb.2013.11.002.
- 1271 61. Bergert M, et al. (2015) Force transmission during adhesion-independent migration. *Nat Cell Biol* 17(4):524–9.
- 1272 62. Liu Y-J, et al. (2015) Confinement and low adhesion induce fast amoeboid migration of slow mesenchymal cells. *Cell* 160(4):659–672.
- 1273 63. Ostrowski PP, Grinstein S, Freeman SA (2016) Diffusion Barriers, Mechanical Forces, and the Biophysics of Phagocytosis. *Dev Cell* 38(2):135–46.
- 1274 64. Sakamoto S, et al. (2018) mDia1/3 generate cortical F-actin meshwork in Sertoli cells that is continuous with contractile F-actin bundles and indispensable for spermatogenesis and male fertility. *PLoS Biol* 16(9):e2004874.
- 1275 65. Levi S, Polyakov M V, Egelhoff TT (2002) Myosin II dynamics in Dictyostelium: determinants for filament assembly and translocation to the cell cortex during chemoattractant responses. *Cell Motil Cytoskeleton* 53(3):177–88.
- 1276 66. Veltman DM, Keizer-Gunnink I, Haastert PJM Van (2009) An extrachromosomal, inducible expression system for Dictyostelium discoideum. *Plasmid* 61(2):119–125.
- 1277 67. Schneider N, et al. (2003) A Lim protein involved in the progression of cytokinesis and regulation of the mitotic spindle. *Cell Motil Cytoskeleton* 56(2). doi:10.1002/cm.10139.
- 1278 68. Linkner J, Nordholz B, Junemann A, Winterhoff M, Faix J (2012) Highly effective removal of floxed Blasticidin S resistance cassettes from Dictyostelium discoideum mutants by extrachromosomal expression of Cre. *Eur J Cell Biol* 91(2):156–60.
- 1279 69. Ran FA, et al. (2013) Genome engineering using the CRISPR-Cas9 system. *Nat Protoc* 8(11):2281–2308.
- 1280 70. Ramalingam N, et al. (2010) Phospholipids regulate localization and activity of mDia1 formin. *Eur J Cell Biol* 89(10):723–732.
- 1281 71. Spudich JA, Watt S (1971) The regulation of rabbit skeletal muscle contraction. I. Biochemical studies of the interaction of the tropomyosin-troponin complex with actin and the proteolytic fragments of myosin. *J Biol Chem* 246(15):4866–71.
- 1282 72. Troll H, et al. (1992) Purification, functional characterization, and cDNA sequencing of mitochondrial porin from Dictyostelium discoideum. *J Biol Chem* 267(29):21072–9.
- 1283 73. de Hostos EL, Bradtke B, Lottspeich F, Guggenheim R, Gerisch G (1991) Corin, an actin binding protein of Dictyostelium discoideum localized to cell surface projections, has sequence similarities to G protein beta subunits. *EMBO J* 10(13):4097–104.
- 1284 74. Small JV, Rottner K, Hahne P, Anderson KI (1999) Visualising the actin cytoskeleton. *Microsc Res Tech* 47(1):3–17.
- 1285 75. Svitkina TM (2009) Imaging Cytoskeleton Components by Electron Microscopy. *Methods in Molecular Biology (Clifton, N.J.)*, pp 187–206.
- 1286 76. Dielweid S, et al. (2010) Mechanical Properties of Bare and Protein-Coated Giant Unilamellar Phospholipid Vesicles. A Comparative Study of Micropipet Aspiration and Atomic Force Microscopy. *Langmuir* 26(13):11041–11049.
- 1287 77. Schindelin J, et al. (2012) Fiji: an open-source platform for biological-image analysis. *Nat Methods* 9(7):676–682.
- 1288 78. Thielicke W, Stamhuis EJ (2014) PIVlab – Towards User-friendly, Affordable and Accurate Digital Particle Image Velocimetry in MATLAB. *J Open Res Softw* 2. doi:10.5334/jors.bl
- 1289 79. Auferheide KJ, Janetopoulos C (2016) Migration of Dictyostelium discoideum to the Chemoattractant Folic Acid. *Methods in Molecular Biology (Clifton, N.J.)*, pp 25–39.